Atomistic simulation of defect-induced amorphization of binary lattices

Horngming Hsieh* and Sidney Yip
Department of Nuclear Engineering, Massachusetts Institute of Technology, Cambridge, Massachusetts 02139
(Received 19 December 1988)

Crystal-to-amorphous transitions are studied by molecular-dynamics simulations in which self-interstitials are randomly and sequentially inserted into solids composed of two atomic species with size difference of 20%. Lennard-Jones interatomic potentials are used for the simulations at finite temperature (about $\frac{1}{4}$ melting) and constant pressure ($P=0$). Two initial structures are considered, an A_3B ordered lattice and an AB solid solution which is significantly disordered. A variety of physical properties are evaluated to assess the effects of the interstitial insertions and subsequent system relaxation. Results provide atomistic details which point to the dominant role of chemical ordering in the amorphization process; they also reveal, in quantitative terms, the essential difference between the amorphization of binary systems and that of single-component lattices studied previously.

I. INTRODUCTION

In recent years it has been found that amorphous solids can be produced by a variety of processes other than the rapid solidification of a melt. In particular, atomic disordering of crystalline solids by irradiation has become a prominent process having considerable fundamental as well as technological interest.[1,2] In the process of rapid solidification, which we might call "vitrification," the system goes from a liquid state to a glassy state when crystallization is suppressed. In the irradiation process, which we will call "amorphization," the system goes from a crystalline state to a glassy state if the lattice is destabilized and recrystallization cannot occur. In the context of fundamental understanding of the glass transition, it is relevant to ask what is the nature of the driving force in vitrification and in amorphization, and what are the factors that determine the threshold condition for each process.

Atomistic simulation is a method by which a fluid system can be quenched practically instantaneously and its subsequent behavior observed on a microscopic time scale. Studies of supercooled fluids and the liquid-to-glass transition have been carried out using this approach,[3,4] although it is still somewhat of an open question how are the simulation results to be related to laboratory measurements which occur on much slower temporal scales. Since simulation offers the advantage of being able to probe a variety of physical properties under conditions which can be characterized precisely, it may be argued that this type of information is invaluable in achieving a better understanding of how amorphous states are produced. The same argument is also applicable to the study of crystal-to-glass transition; here even less is known since only a few simulations have been attempted.[5–8]

In this paper we describe a molecular-dynamics study of amorphization of atomic lattices induced by the rapid introduction of self-interstitials while the system is maintained at constant temperature and pressure. In an earlier work dealing with a monatomic fcc lattice with Lennard-Jones interatomic interaction,[6,9] we have shown that the threshold condition for defect-induced amorphization is both rate and concentration dependent. The present work is an extension to binary lattices in which the only difference between the two atomic species is the particle size. We find that the existence of two atomic species has a profound effect on the nature of structural ordering, and that for a certain choice of the size disparity between the species, the threshold requirements for amorphization of a binary system are considerably reduced compared to those for a monatomic solid. An analogous behavior is known in simulations of vitrification where binary fluids are found to be much more resistant to crystallization than their monatomic counterparts.[10]

Our simulation results also reveal the presence of residual stresses as a result of the size disparity. The distribution of the hydrostatic stress changes significantly upon structural disordering, which is an indication that local stresses can play an important role in the amorphization process. Another manifestation of the correlation of mechanical behavior with structural order is the change in elastic constants upon amorphization, a reduction in C_{11}, an increase in C_{12}, and a drastic reduction in C_{44}. This behavior is quite general since similar changes are also observed in the case of the monatomic lattice.

The present work is part of an attempt to understand radiation-induced amorphization in terms of the disordering effects of point defects.[5] While there exists a considerable body of data on both electron and ion irradiations,[1,2] there are few models to provide a theoretical basis for investigating the role of defects in the amorphization process.[11] Simulation results can be useful in this respect. Recently, it has been found that a glassy phase can be formed in a crystalline lattice containing grain boundaries[7] and that a model binary alloy in an initially fully disordered structure can become amorphous upon relaxation.[8]

II. MOLECULAR-DYNAMICS SIMULATION MODELS

In this study the standard molecular-dynamics method[5] is applied to a periodic system of two types of particles, A and B, which are distinguished only by their interaction potentials. The potentials are of the Lennard-Jones (6-12) form,

$$V_{\alpha\beta}(r)=4\varepsilon_{\alpha\beta}[(\sigma_{\alpha\beta}/r)^{12}-(\sigma_{\alpha\beta}/r)^{6}] , \tag{1}$$

where $\alpha,\beta = A$ or B. For the parameters of the three interactions, V_{AA}, V_{BB}, and V_{AB}, we take

$$\begin{aligned} &\varepsilon_{AA}=\varepsilon_{BB}=\varepsilon_{AB}\equiv\varepsilon , \\ &\sigma_{AA}=\sigma_{BB}/1.2 , \\ &\sigma_{AB}=(\sigma_{AA}+\sigma_{BB})/2\equiv\sigma . \end{aligned} \tag{2}$$

Thus, with the well depths for all three potentials taken to be the same, particles A and B differ only in their size (B is larger by 20%), and the geometric mean is used as the size parameter for the A-B interaction (Lorentz-Berthot combining rule). Notice also we do not consider any mass difference between the two species.

For the equations of motion we adopt a Lagrangian formulation[12] and use a fifth-order predictor-corrector algorithm to carry out the integration. In this method the simulation cell is allowed to change shape and volume in response to an external stress, which we will set equal to zero in all the simulation runs. All physical quantities are expressed in dimensionless forms, length in unit of σ, energy in ε, pressure in ε/σ^3, and time in $\tau\equiv(m\sigma^2/\varepsilon)^{1/2}$, m being the particle mass. For operational details, we note here that the interparticle force is cut off at $r_c=2.33$, the time-step size Δt is 0.01, and the system temperature is maintained constant by velocity rescaling whenever the instantaneous temperature exceeds a certain tolerance limit.

A simulation run consists of four stages, equilibration of the fcc binary lattice prior to any defect introduction, insertion of self-interstitials sequentially at a certain rate, continued simulation without further particle insertion, and a second period of simulation without perturbation. From the first stage one obtains the properties of the unperturbed or reference system. The second stage is the perturbation or "irradiation" phase. The third is the relaxation or "annealing" phase, and the results from the fourth stage provide a check that the third stage has been run long enough.

To insert self-interstitials we choose an atom at random and find among its nearest neighbors three which are also first neighbors to each other. The positions of these three particles relative to the chosen atom are taken to be vectors $\mathbf{a},\mathbf{b},\mathbf{c}$ such that the position for the interstitial is given by $(\mathbf{a}+\mathbf{b}+\mathbf{c})/2$. When the lattice is not severely distorted, this procedure locates the octahedral position at the center of the fcc unit cell. When many interstitials have been inserted, it can happen that the procedure fails to locate an interstitial position relative to an atom. In such cases the simulation would continue with the choice of another atom. Immediately after a new particle is inserted, the simulation time step is reduced to 0.05 of the normal time-step size to allow for local relaxation of the crowding effects of the insertion. The time-step size is then gradually increased back to its normal value over the next 20 steps.

The defect-insertion stage ends when a certain number of interstitials, N_i, has been introduced. The second stage is therefore characterized by N_i and an interstitial insertion rate r_i. We will consider two insertion rates, $r_i=5.95$ and 14.71, where r_i^{-1} is the time interval, in units of τ, between insertions. In each case the simulation continues through all four stages at the same temperature and pressure. Particle trajectories during each stage are saved and cumulative averages are computed separately for each stage.

We have studied two binary solids with different initial structures: one is an A_3B lattice and the other an AB solid solution. In the former, particles occupying the corner sites of a fcc unit cell are assigned to be type B, while those on the face sites are type A, and in the latter structure species A and B have equal probability of occupying each site in the fcc lattice. Each system contains $N=576$ particles at the start of the simulation and during stage 1 it is equilibrated at $T^*=k_BT/\varepsilon=0.2$ (about 0.3 of melting) and zero pressure.

In presenting the results of the simulations, we will first consider the characteristic temporal responses during each of the four stages. Then we will examine the changes in structural and mechanical properties brought about by the interstitial insertion and subsequent relaxation processes. Table I shows three simulation series which we have carried out, each corresponding to a particular combination of initial structure and insertion rate. In these cases stage 1 is equilibration without defect for a period of 10^3 time steps, stage 2 is the insertion of 40 interstitials, stage 3 is the system relaxation for 3000 steps, and stage 4 is further relaxation for 2000 steps.

The system response in the density, average potential energy per atom, static structure factor, and an order factor (defined below) are given in Table I. These are average values calculated over a portion of the trajectories near the end of each stage. The density is obtained as the ratio of the number of particles in the system at the given time to the instantaneous volume of the simulation cell which is given by $\mathbf{h}_1\cdot\mathbf{h}_2\times\mathbf{h}_3$, $\mathbf{h}_i$ being the basis vectors defining the simulation cell.[12] The static structure factor and order factor are defined as

$$S(\mathbf{K})=(1/N)\left|\sum_{j=1}^{N}\exp(i\mathbf{K}\cdot\mathbf{r}_j)\right|^2 , \tag{3}$$

$$\rho(\mathbf{K})=(1/N)\sum_{j=1}^{N}\cos(\mathbf{K}\cdot\mathbf{r}_j) , \tag{4}$$

where $\mathbf{K}$ is a reciprocal-lattice vector chosen along the closed-packed direction, $\mathbf{K}=(2\pi/L_z)(n,n,n)$, L_z being the length of the simulation cell along the z or [111] direction. Several $|\mathbf{K}|$ values are considered in each calculation; the values of $S(\mathbf{K})$ and $\rho(\mathbf{K})$ shown in Table I

TABLE I. System responses after insertion of 40 interstitials obtained from simulations with different initial structures and insertion rates r.

Series	Struct.	Rate r	Stage	Density	$-U$	$S(\mathbf{K})$	$\rho(\mathbf{K})$
E	A_3B	5.95	1	1.12	7.08	520	0.95
			2	1.06	6.75	100	0.40
			3	1.09	6.95	10	0.15
			4	1.09	6.97	8	0.11
F	A_3B	14.71	1	1.12	7.08	520	0.95
			2	1.04	6.55	150	0.50
			3	1.09	6.95	20	0.15
			4	1.09	6.99	5	0.08
D	AB	14.71	1	0.97	6.95	210	0.60
			2	0.92	6.60	70	0.35
			3	0.95	6.90	5	0.10
			4	0.95	6.91	7	0.10

correspond to values of $|\mathbf{K}|$ for which $S(\mathbf{K})$ is a maximum. A comparison of the results in Table I for series E and F shows only slight variation with insertion rate. Since this is true for all the properties that we will discuss in Sec. III, we will not consider series E any further.

III. STUDY OF A_3B ORDERED LATTICE

The significance of the system responses shown in Table I will become clear once we consider the time-dependent behavior of the properties at each stage. For an overview of the effect of interstitial insertion, we show in Fig. 1 two projections of the particle configurations before interstitial insertion, after 20 insertions, and after 40 insertions. In a qualitative way the results suggest a certain structural coarsening or the appearance of local-density inhomogeneities in the system.

Figure 2 shows the density variation during each of the four stages. The oscillatory behavior during stage 1 is caused by vibratory motions of the simulation cells, a characteristic of the equations of motion for the $\mathbf{h}_i$ vectors which is of no physical interest. When interstitials are inserted, the density is seen to decrease monotonically. This implies that the instantaneous volume expansion of the cell is greater than the volume needed to accommodate the new particle at the original density. From previous studies of amorphization of one-component crystals, we have found that the decrease of density with interstitial insertion levels off after about 80–100 insertions, and this behavior can be associated with the formation of new (111) planes as new particles are added to the system.[6]

When the system is allowed to relax after insertion of 40 interstitials, there is a rapid recovery of density. However, the original value of the density is not obtained, which implies that the packing of the particles has been altered significantly. Since no further change is seen during stage 4, one can also conclude that density relaxation during stage 3 is more or less complete.

Figure 3 shows the variation of the average potential energy per atom. The presence of the interstitials raises the energy level of the system, as can be seen from the stage-2 behavior. Once the insertion stops, there is a rapid response in energy relaxation. As in the case of the density, the recovery is not complete and the system is left in an excited state relative to the unperturbed lattice.

Figure 4 shows the mean-squared displacement which is defined as

$$\Delta^2 r = (1/N) \sum_{i=1}^{N} [\mathbf{r}_i(t) - \mathbf{r}_i(0)]^2 . \tag{5}$$

Prior to particle insertion, this quantity gives a measure of the average thermal vibrational amplitude of the particles; it is seen to be quite small compared to the variations during particle insertions and subsequent relaxation. During insertion the displacement function increases more or less linearly, which is not unexpected since there must be significant local rearrangements following every interstitial introduction. During relaxation the displacement increases even more strongly, which means that the rearrangements are even more active during this phase. Since stage 4 shows only a slight increase, one can conclude that the simulation has run long enough.

The structural response of the system is depicted in Figs. 5 and 6. The loss of crystalline order during particle insertion is to be expected, but, unlike the density and the potential-energy responses, during relaxation there is continued disordering instead of recovery. It is noteworthy that the latter disordering is apparently associated with the large particle displacements observed in Fig. 4(c). The results from stage 4 indicate that further change is unlikely, which is consistent with the other responses.

The radial distribution function $g(r)$ is defined to be

$$g(r) = (1/4\pi N r^2 \delta r) \sum_{i,j=1}^{N}{}' \int_{r}^{r+\delta r} dr' \, \delta(r_{ij} - r') . \tag{6}$$

Three distributions are shown in Figs. 7–9: the total distribution function $g_t(r)$, the distribution $g_{BB}(r)$ of B-type particles relative to a B particle at the origin, and the distribution $g_{AB}(r)$ of B relative to an A particle, respectively. Also shown in each case is the cumulative distribution

$$G(r)=\int_0^r dr' 4\pi(r')^2 g(r') . \quad (7)$$

Since particle species are not distinguished in $g_t(r)$, one sees in Fig. 7 the behavior appropriate to a one-component system. From stage 1 the distribution shows the first four neighbors in a fcc lattice, with $G(r)$ giving the first three coordination numbers at 12, 6, and 24. It may seem that the second-, third-, and fourth-neighbor peaks have not been smeared out during stage 2; this appearance is mostly caused by the contributions from the early configurations, which contain only a few interstitials and the lattice was effectively still crystalline. The shape of $g(r)$ obtained from the relaxation stage is reminiscent of a liquid. Note, in particular, the absence of the second-neighbor peak of a fcc lattice and a second max-

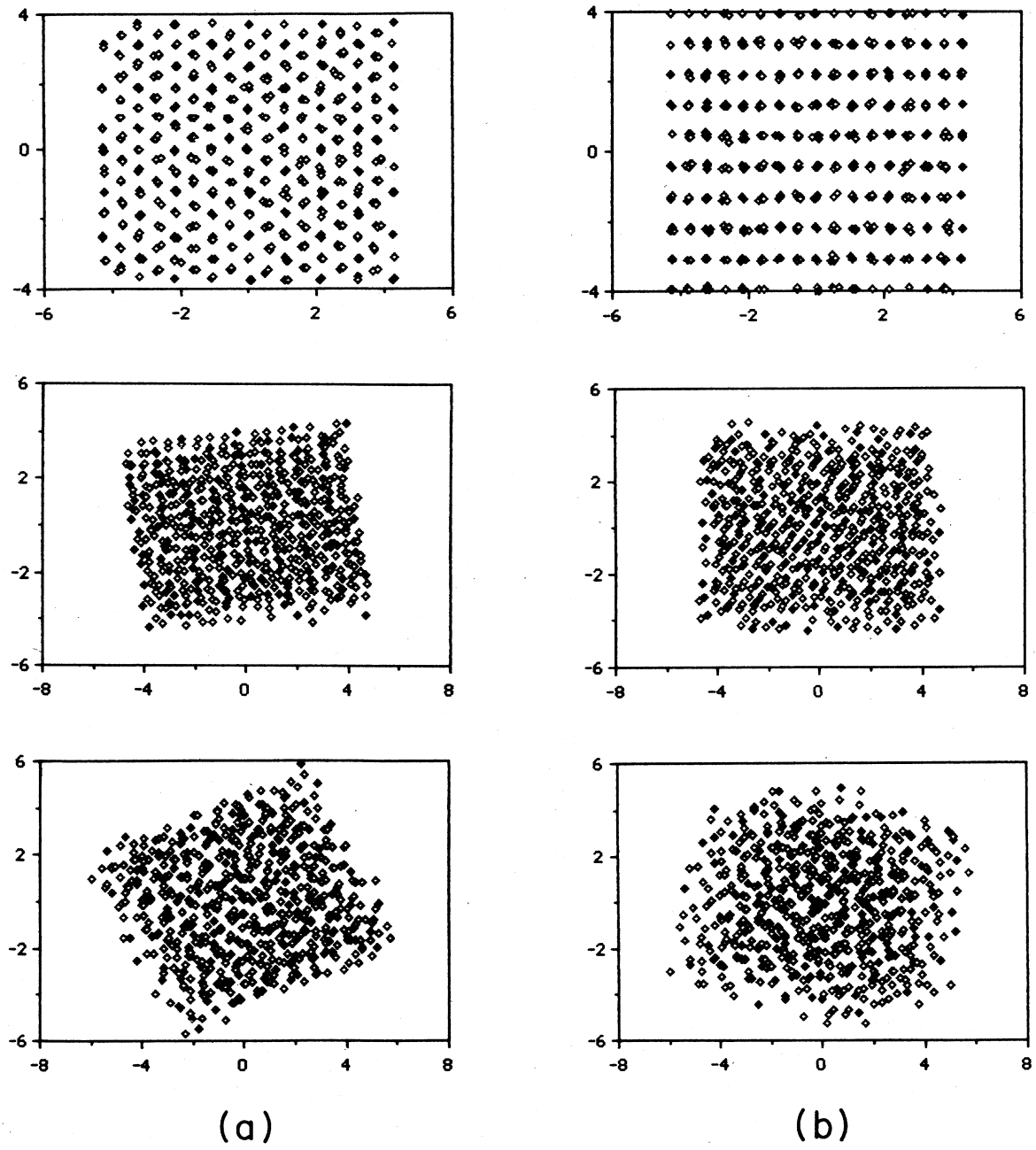

FIG. 1. (a) xy projection of atomic positions after insertion of a number, N_i, of interstitials into an ordered A_3B lattice at $T^*=0.2$, $P^*=0$, and fast insertion rate (series F); $N_i=0$ (top), 20 (middle), and 40 (bottom). Open and solid symbols denote atom species A and B, respectively. (b) Same as (a), except projection is xz.

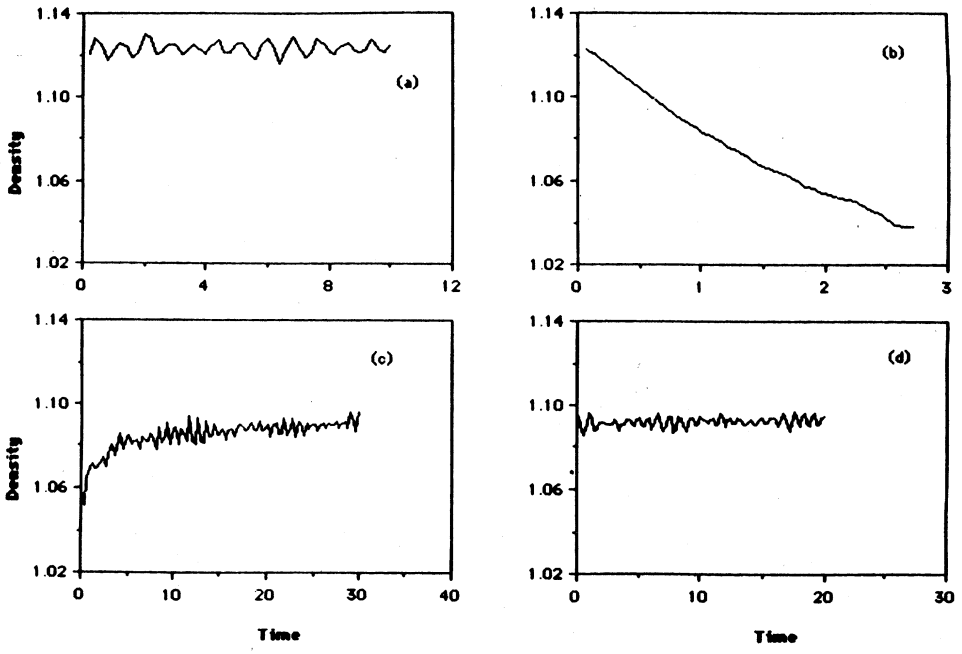

FIG. 2. Time response of system density during the four stages of simulation (series F) of interstitial insertion and relaxation. (a) Thermal equilibration of A_3B ordered lattice, (b) insertion of $N_i=40$ interstitials, (c) relaxation with no further interstitial insertion, and (d) further relaxation. Time scales are one unit equals 10^2 time steps in (a), (c), and (d), and one unit equals about 200 time steps in (b). Entire simulation is carried out at $T^*=0.2$ and $P^*=0$.

imum in $g(r)$ replacing the previous third- and fourth-neighbor peaks. This behavior has been observed in the study of the one-component lattice.[6]

The distribution $g_{BB}(r)$ is quite different from $g_t(r)$ in the A_3B lattice. As seen in Fig. 8(a), $g_{BB}(r)$ has only two peaks, one at the second-neighbor position and the other at the fourth-neighbor position. The extent to which these two peaks are smeared out is difficult to tell from Fig. 8(b) because of the contributions of the early configurations. One suspects that at the end of the inser-

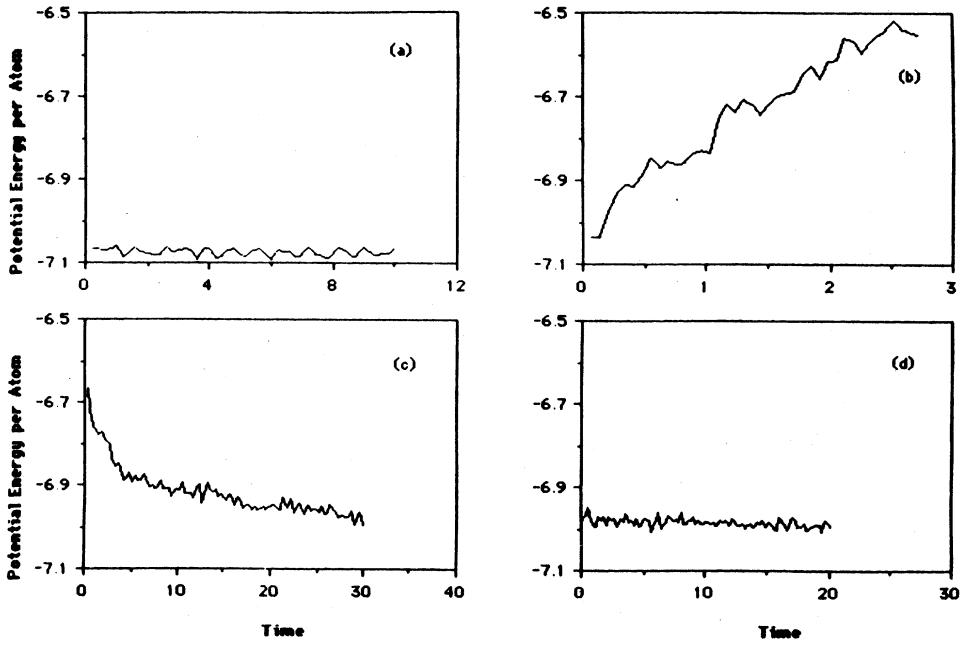

FIG. 3. Same as Fig. 2, except the response is that of potential energy per atom (in units of ε).

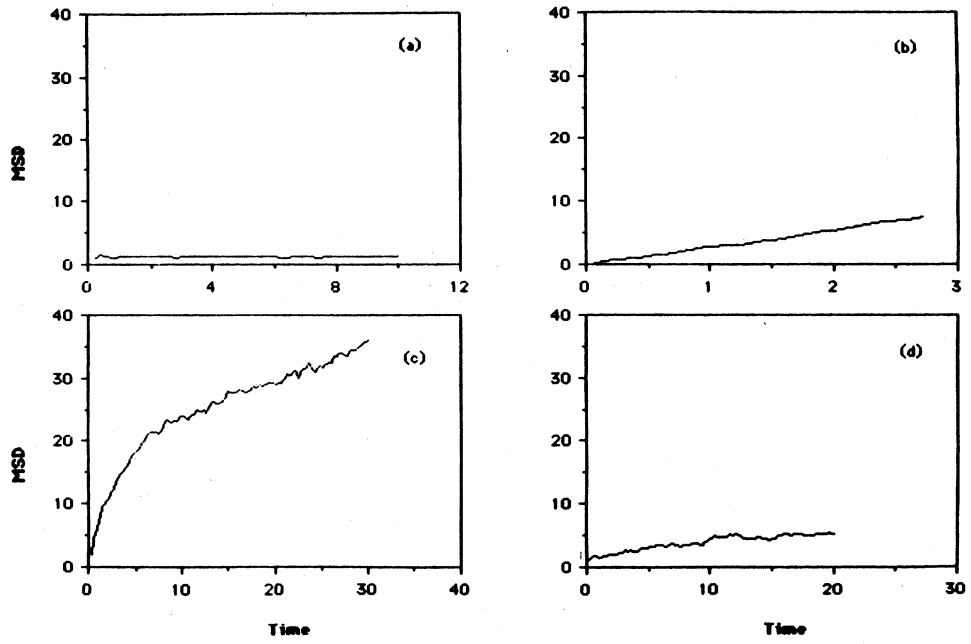

FIG. 4. Same as Fig. 2, except the response is that of mean-squared displacement of all the atoms. Unit of $\Delta^2 r$ (MSD) is $0.01\sigma^2$.

tion stage g_{BB} must be closer to Fig. 8(c) than anything else. In Fig. 8(c) one has essentially a completely different structure from Fig. 8(a); the distribution now is quite similar to $g_t(r)$.

The cross correlation $g_{AB}(r)$ also differs from $g_t(r)$ initially, but its transformation is less drastic by comparison to g_{BB}. As shown in Fig. 9(a), the A_3B lattice gives a peak in $g_{AB}(r)$ at the nearest-neighbor position with the expected coordination number of 4, and another peak at the third-neighbor position with coordination number 8. After insertion and relaxation, $g_{AB}(r)$ also tends to a distribution similar to that of $g_t(r)$ and $g_{BB}(r)$.

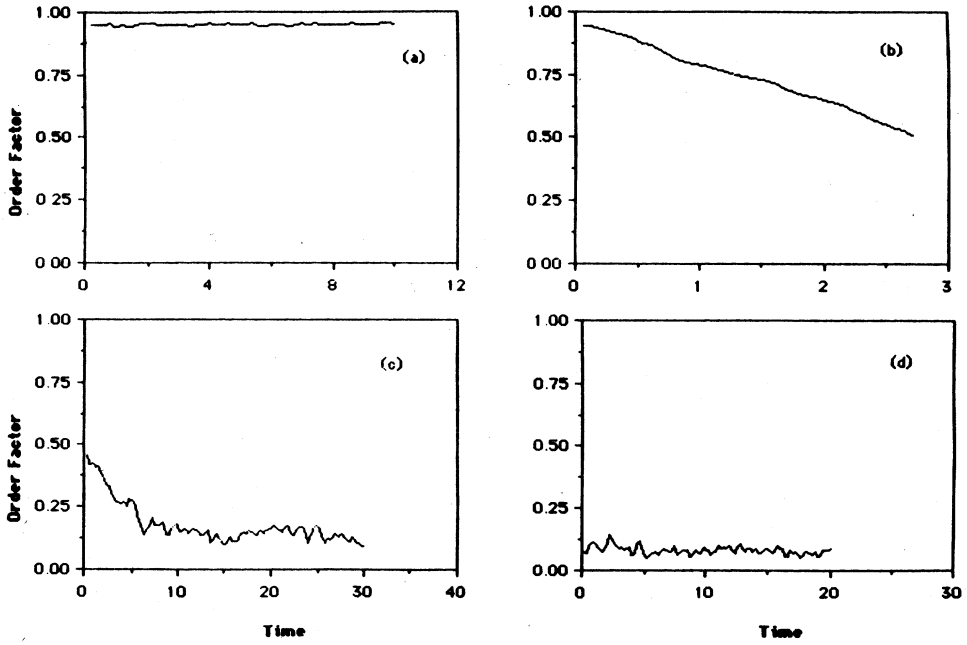

FIG. 5. Same as Fig. 2, except the response is that of the order factor $\rho(\mathbf{K})$, with $\mathbf{K}=(2\pi/L_z)(0,0,n)$, with n chosen to give the maximum value of $S(\mathbf{K})$.

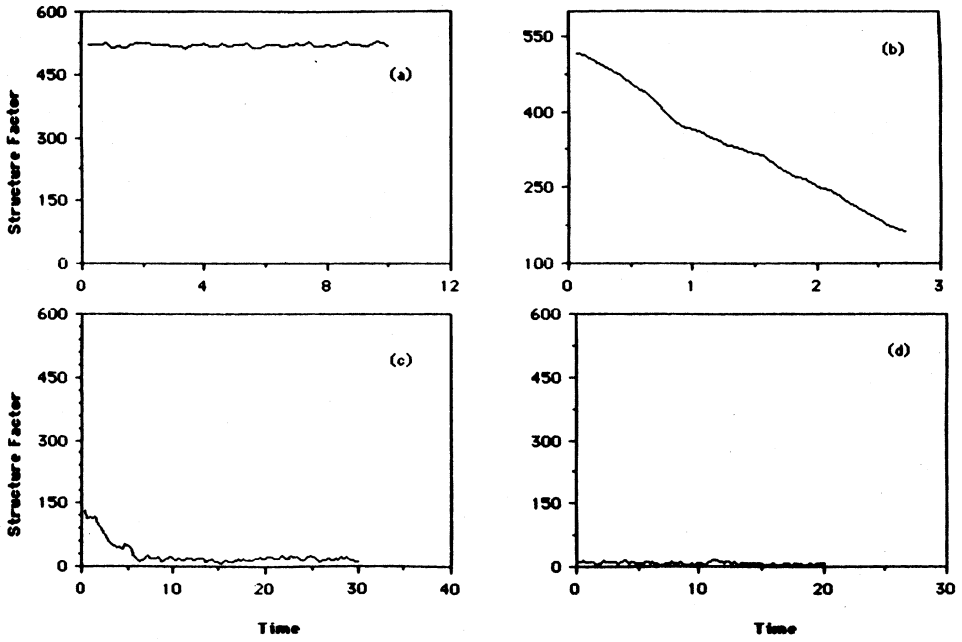

FIG. 6. Same as Fig. 2, except the response is that of the static structure factor $S(\mathbf{K})$.

Atomic configurations can be characterized by Voronoi polyhedra, the construction of which leads to quantitative measures of the volume associated with each atom and the topology of its nearest neighbors. We have developed a program to compute these polyhedra given an arbitrary collection of particle positions. Figure 10 shows the fractional distributions of the Voronoi volumes of A and B particles. In the ordered lattice there is only a slight difference between the two distributions. As a result of interstitial insertion, the difference becomes considerably greater; polyhedron volumes of the larger species are decidedly larger. This suggests that as the lat-

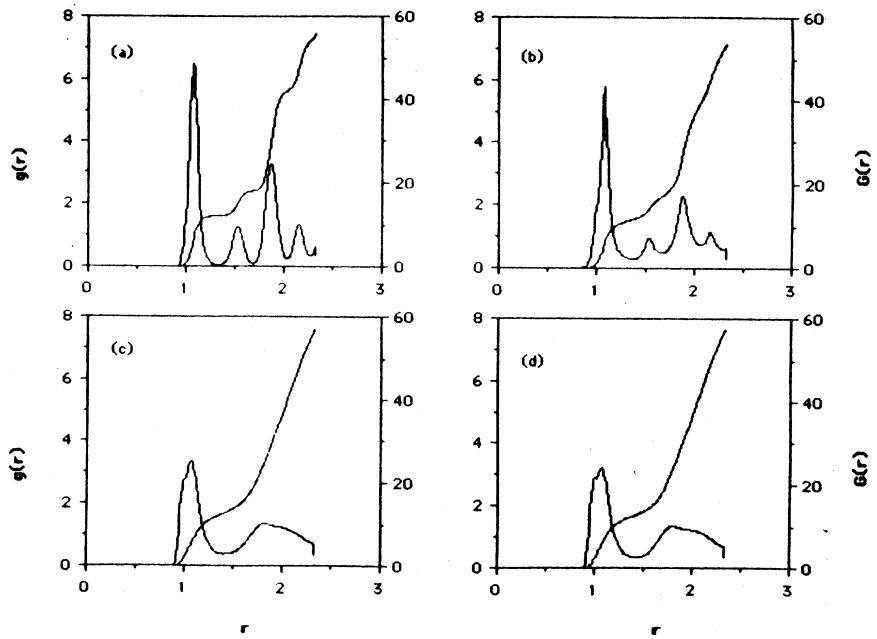

FIG. 7. Radial distribution function $g_t(r)$ and corresponding cumulative distribution $G_t(r)$ for the four stages of simulation (series F) of interstitial insertion and relaxation; (a) equilibration of A_3B ordered lattice, (b) insertion of 40 interstitials, (c) relaxation with no further interstitial insertion, and (d) further relaxation. All results are averages over contributions calculated periodically during each stage. Reduced distance is in units of σ.

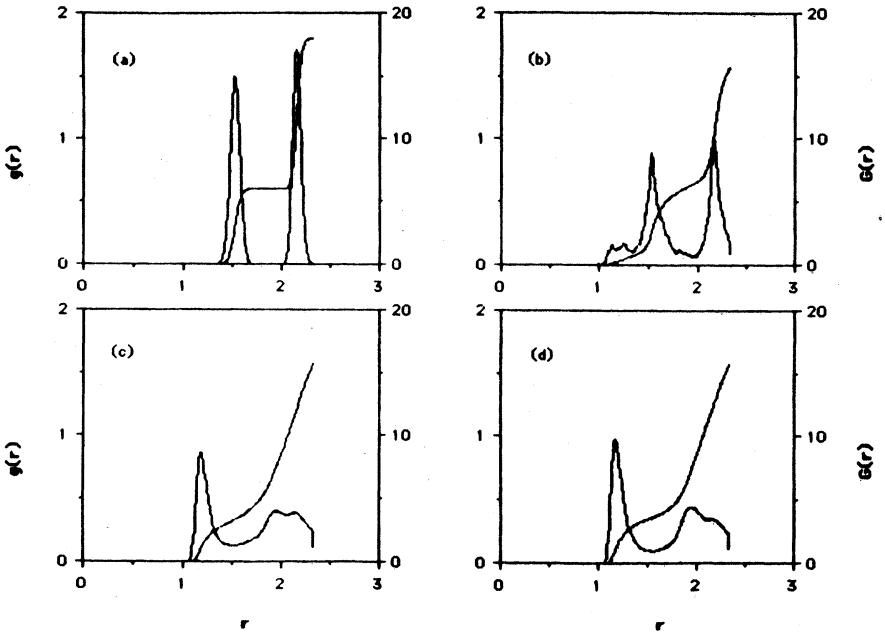

FIG. 8. Same as Fig. 7, except the distribution function is $g_{BB}(r)$.

tice structure is destroyed the volume distribution becomes governed by the particle size as one would expect in a disordered environment. Figure 11 shows the distributions of the number of faces of the Voronoi polyhedra. Again, one sees that after insertion and relaxation the distributions separate, with the polyhedra for the larger particles having more faces.

Another measure of local variations in particle arrangements is the atomic-level stress,[12] defined by the second-rank tensor

$$\sigma_i=(1/\Omega_i)\left[m_i\mathbf{v}_i\mathbf{v}_i-\sum_{j\,(\neq i)}(V'_{ij}/r_{ij})\mathbf{r}_{ij}\mathbf{r}_{ij}\right], \tag{8}$$

where Ω_i is the volume of atom i. In this study the local stresses are transformed into principal stresses, σ_1, σ_2, and σ_3, which are then used to obtain the hydrostatic stress,

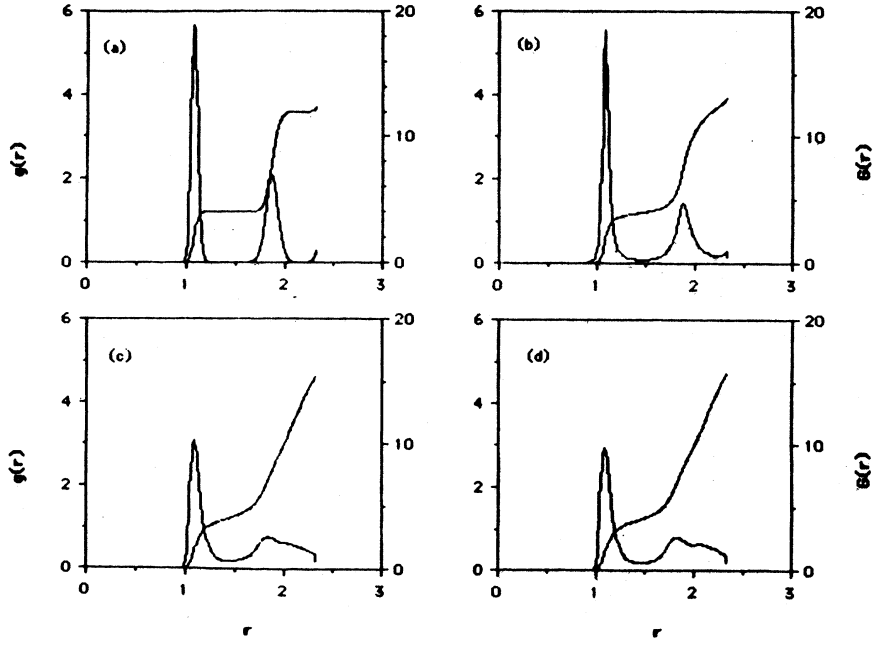

FIG. 9. Same as Fig. 7, except the distribution function is $g_{AB}(r)$.

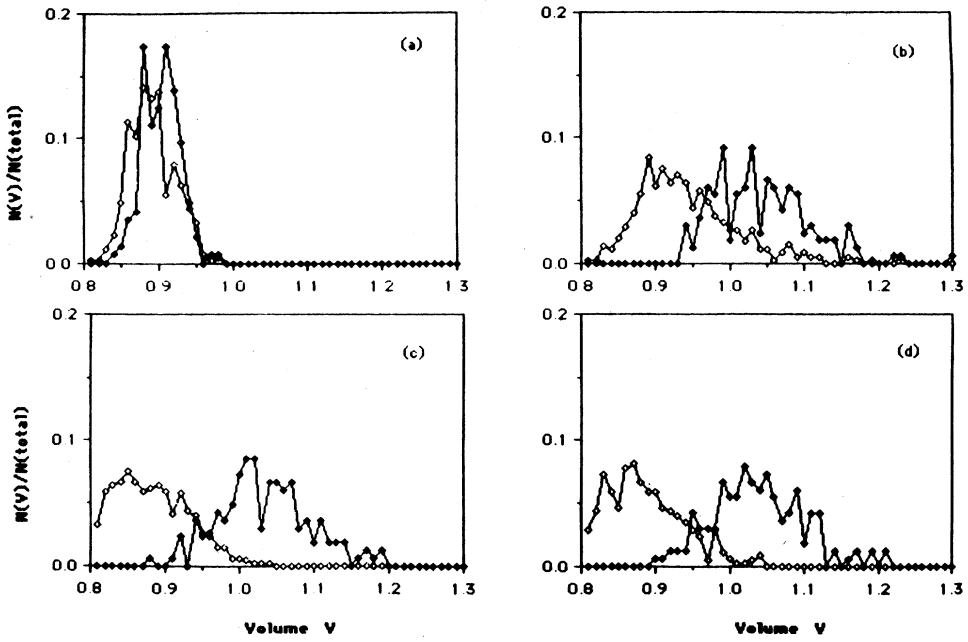

FIG. 10. Normalized distribution of volume of Voronoi polyhedra for the four stages of simulation (series F, see Fig. 7). Open and solid symbols denotes atom species A and B, respectively. Reduced volume is in units of σ^3.

tain the hydrostatic stress,

$$P=(\sigma_1+\sigma_2+\sigma_3)/3\ , \tag{9}$$

and the von Mises shear stress,[13]

$$s=\{[(\sigma_1-\sigma_2)^2+(\sigma_2-\sigma_3)^2+(\sigma_3-\sigma_1)^2]/6\}^{1/2}\ . \tag{10}$$

Figure 12 shows the distributions of the hydrostatic stresses acting on the two species. In the ordered lattice the larger particles (B) are subjected to a compressive stress, while the smaller particles (A) experience a slight tensile stress. After insertion and relaxation, both species experience the same distribution, which is now centered about zero stress.

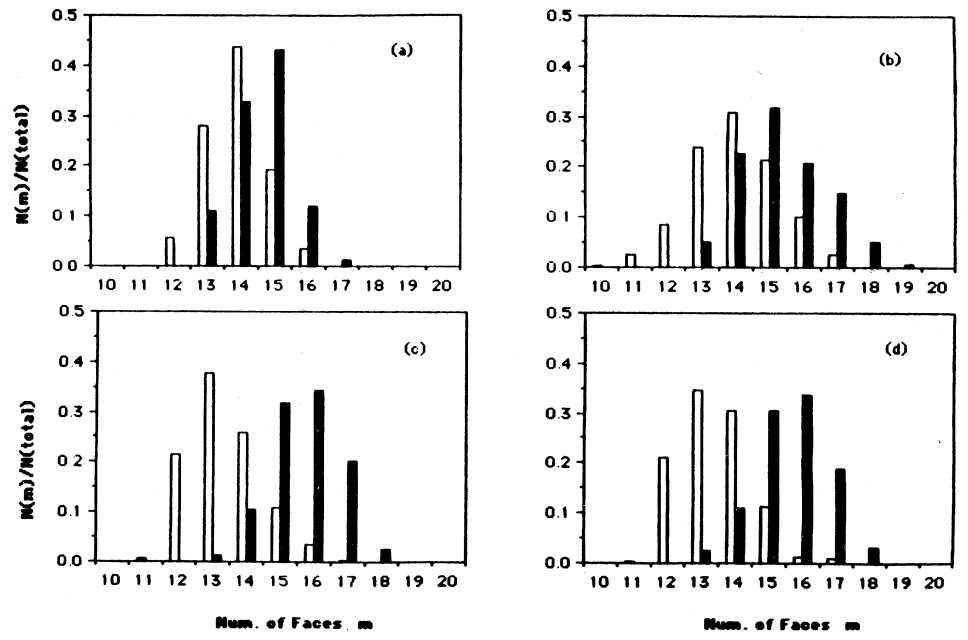

FIG. 11. Same as Fig. 10, except the normalized distribution is that of number of faces of the Voronoi polyhedra.

The mechanical properties of a solid can be measured in terms of elastic constants that can be calculated using fluctuation formulas.[14] The adiabatic elastic constants, under the condition of zero external stress, are given by

$$C_{ijkl}=(2N/\beta\Omega)(\delta_{ik}\delta_{jl}+\delta_{il}\delta_{jk})-\Omega\beta\delta(\pi_{ij}\pi_{kl})+(1/\Omega)\left\langle \sum_{\alpha,\gamma}(V''/r^2-V'''/r^3)r_i r_j r_k r_l \Big|_{r=r_{\alpha\gamma}} \right\rangle , \tag{11}$$

where $\beta=1/k_B T$, and $\delta(\pi_{ij}\pi_{kl})=\langle \pi_{ij}\pi_{kl}\rangle-\langle \pi_{ij}\rangle\langle \pi_{kl}\rangle$. The elastic-constant results are given in Table II, where the contributions from the three terms in Eq. (12) are shown separately. It is seen that the kinetic contribution is small, fluctuations in the stress tensor give a negative contribution, and the Born terms dominate. After insertion and relaxation, there is an appreciable decrease in C_{11}, an increase in C_{12}, and a sharp reduction in C_{44}. It is seen also that these changes mainly occur as a result of the greater fluctuations in the stress tensor.

An overall characterization of the vibrational properties of the system is provided by the generalized frequency distribution $f(\omega)$, which can be calculated as the

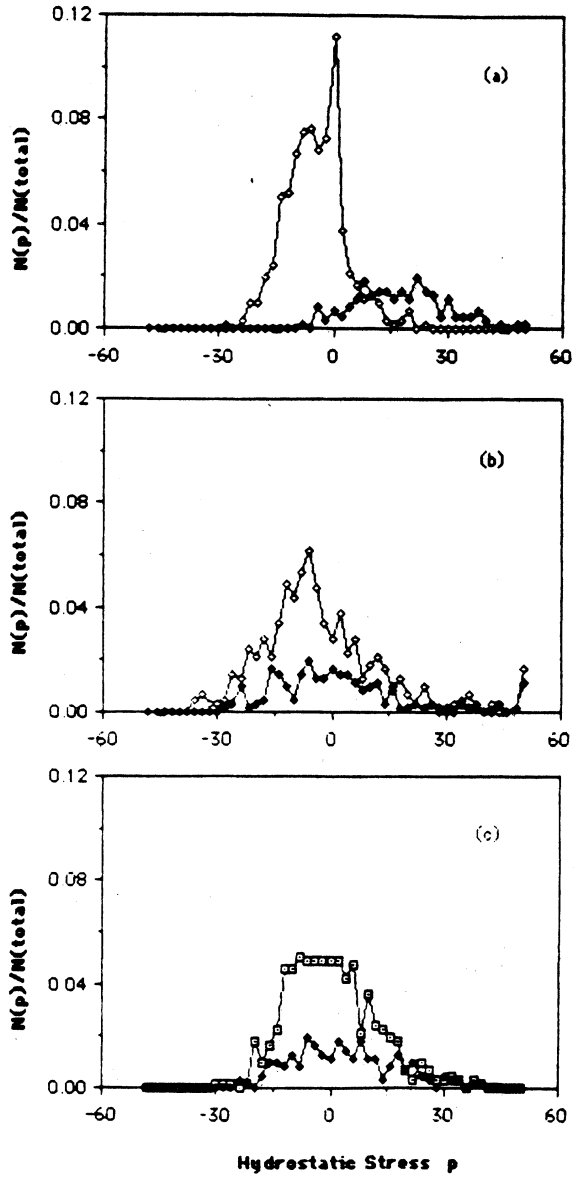

FIG. 12. Normalized distribution of hydrostatic stress P for the first three stages of series-F simulation. Results are averages over each stage. Open and solid symbols denote atom species A and B, respectively.

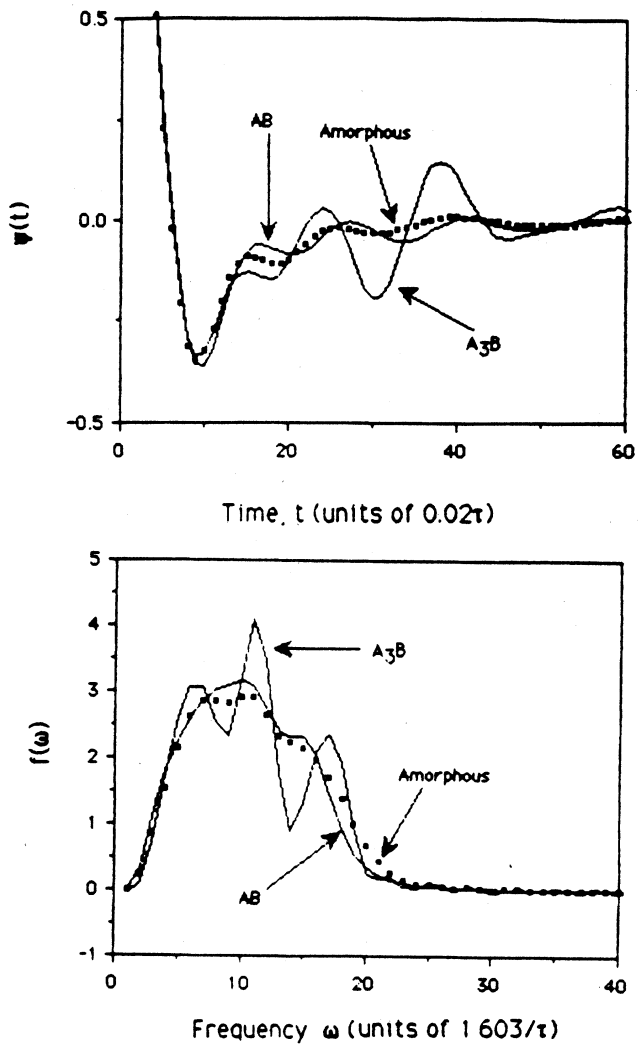

FIG. 13. Velocity autocorrelation function $\psi(t)$ and its Fourier transform $f(\omega)$ of A_3B lattice (series E, stage 1), AB solution (series D, stage 1), and amorphized solid (series F, stage 4).

TABLE II. Elastic constants of an amorphized A_3B solid obtained from simulation series F, stage 4. Contributions from the three terms in Eq. (11)—kinetic, fluctuation, and Born terms, respectively—are shown separately. Shown on the second line of each entry are the corresponding values for the A_3B lattice without defects, simulation series F, stage 1.

	C_{11}	C_{22}	C_{33}	C_{12}	C_{13}	C_{23}	C_{44}	C_{55}	C_{66}
Kinetic	4.0	4.0	4.0	0	0	0	2.0	2.0	2.0
	4.0	4.0	4.0	0	0	0	2.0	2.0	2.0
Fluctuation	−191	−185	−198	39.4	75.8	62.4	−126	−129	−127
	−101	−84.8	−95.7	−20.7	−3.51	-22.9	−21.8	−26.5	−23.6
Born	491	504	502	168	162	159	159	162	168
	552	552	551	142	142	142	142	142	142
Total	303	323	308	221	207	238	34.8	35.1	43.0
	456	471	460	121	107	119	122	118	120
Average		311			222			38	
		462			116			120	

Fourier transform of the velocity autocorrelation function,[15]

$$\psi(t)=\sum_i \langle \mathbf{v}_i(t)\cdot\mathbf{v}_i(0)\rangle \Big/ \sum_j \langle \mathbf{v}_j(0)\cdot\mathbf{v}_j(0)\rangle \ . \qquad (12)$$

Figure 13 shows $\psi(t)$ and its transform $f(\omega)$ for the A_3B ordered lattice prior to interstitial insertion and after insertion and relaxation, along with the results for the AB solid solution prior to interstitial insertion (see Sec. IV). One can discern a slight enhancement of low-frequency distribution in $f(\omega)$ and a somewhat more pronounced increase in the high-frequency end of the distribution as a result of amorphization. These effects are more evident in the study of the one-component system.[9] The low-frequency enhancement is a feature that has been observed in neutron inelastic spectra of metallic glasses.[16]

To complete the discussion of the A_3B system, we show in Fig. 14 a collection of properties calculated after 20 interstitials have been introduced. These intermediate results help to confirm the above interpretations of the system response during stage 2.

In summary, we find that the introduction of interstitials into an initially ordered binary lattice drives the system to a level of disturbance from which it relaxes into an amorphous structure. Unlike the one-component system, which shows an amorphization threshold in the insertion rate, the binary lattice, for the present choice of size disparity, is much less resistant to amorphization. In the computer-simulation studies of the glass transition by quenching a liquid, it is known that nucleation occurs readily in the one-component system but not in the binary system.[4,10] Since we have followed the behavior of different physical properties through the various stages, we are now in a position to give a more complete picture of the process of defect-induced amorphization. This discussion will be undertaken in Sec. V after we consider the study of the AB solid solution in the next section.

IV. STUDY OF AB SOLID SOLUTION

The AB solid solution is constructed by taking a fcc lattice and assigning on a random basis half of the lattice sites to be occupied by type-A particles and the other half by type B. The system is then allowed to relax at the temperature of interest, $T=0.2$ in this study. Because of the size disparity between the two species, a certain amount of disorder is already present in the initial configuration. An indication of this can be seen from the coordination number of the nearest neighbors as obtained from the cumulative distribution function $G(r)$, 12.96, 6.39, 6.60, 6.33, and 6.65 for g_t, g_{AA}, g_{BB}, g_{AB}, and g_{BA}, respectively. For the A_3B ordered lattice without defects, the corresponding values are 12, 8, 0, 4, and 12.

The AB system has been studied under the condition of 40 interstitial insertions at the rate of 14.71 particles per unit time τ, followed by two relaxation stages. Some of the properties obtained from this simulation series are given in Table I. Relative to the results for the A_3B system, there is only a slight decrease in density and increase in potential energy brought about by the interstitial insertion and subsequent relaxation. Even though the AB system is initially more disordered, in the relaxed final state structural disorder in both systems appears to be similar.

For an overview of the particle configurations before and after interstitial insertions, we show in Fig. 15 projections of all the particles in the simulation cell. One can see the system is already quite disordered by the 20% size disparity between the two species. The distortion effect of the interstitials noted in Fig. 1, namely fluctuation in local density, is even more pronounced in this case. The response of $S(\mathbf{K})$, shown in Fig. 16, reveals that some disordering occurs during the insertion stage, but very little change seems to take place during relaxation. The same behavior is indicated by the radial distribution functions $g_t(r)$, given in Fig. 17, and the volume distribution of the Voronoi polyhedra, given in Fig. 18. The distribution of hydrostatic stresses, given in Fig. 19, shows the relief of compression on type-B particles and tension on

type-A particles as a consequence of the interstitial insertion, an effect also observed in the A_3B system.

Elastic constants calculated for the solid-solution system are given in Table III. Relative to the ordered A_3B system, C_{11} and C_{44} are significantly smaller, while C_{12} is larger before the introduction of interstitials. Notice also that there is significant deviation from cubic symmetry. These effects are clearly due to the structural disorder associated with the solid solution. The presence of interstitials causes only a slight change in the various elastic constants, in the direction to be expected.

In summary, we find the AB solid solution studied here to be a system already quite disordered without the introduction of any extrinsic defects, and the effect of inserting a high concentration of interstitials is small but consistent with that observed in the A_3B system.

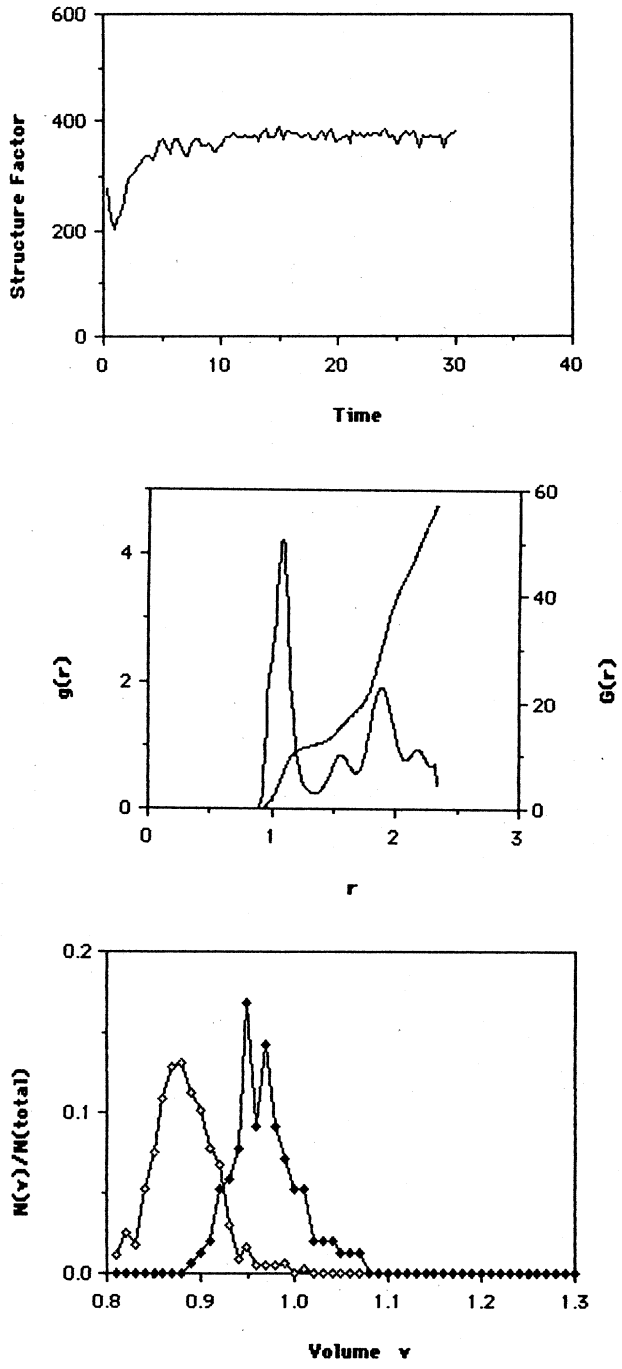

FIG. 14. System responses of A_3B lattice with 20 interstitials inserted at $r=14.71$. Top, time variation of $S(\mathbf{K})$ during stage 3 [compare with Fig. 6(c)], time in units of τ; middle, $g_t(r)$ after stage 3 [compare with Fig. 7(c)]; bottom, distribution of volume of Voronoi polyhedra after stage 3 [compare with Fig. 10(c)].

V. DISCUSSION

By means of molecular-dynamics simulation we have carried out a systematic study of the structural disordering effects of introducing self-interstitials into solids composed of two atomic species. By varying the initial structures and monitoring the evolution of each system through a variety of physical properties, we have obtained a comprehensive collection of results pertaining to the process of defect-induced amorphization. In considering the significance of these results, it is relevant to also refer to similar investigations[5,6,9] of amorphization of a pure element where the effects of chemical ordering are totally absent.

A general behavior of all the systems studied is the overexpansion of the solid when interstitials are first introduced. This density decrease is clearly associated with the disruption of crystalline order as observed through the quantities which measure structural properties, $S(\mathbf{K})$ and $\rho(\mathbf{K})$. In Table I one sees that this correlation between structural order and density also extends to the potential energy; there is an increase in potential energy when the system becomes disordered. One may ask whether the density and potential-energy responses will cease to vary with further defect insertions when the system is totally disordered. Such a leveling off has been observed in simulations on monatomic lattices at higher interstitial concentrations;[5,6,9] we can expect the same behavior in the present study. Further investigation of the correlation between volume expansion and structural disorder can be extremely enlightening in view of the possible existence of a fundamental connection between melting and amorphization.[17] Work along this direction is currently in progress.[18]

Perhaps the most interesting aspect of this study is the role of chemical disorder. We have adopted the simplest model of chemical ordering by assuming the potential functions all have the same well depth and the same mass for particles of both species. This eliminates any preference for particles to associate with one species over the other as well as inertial effects in particle interactions due to mass difference. Any chemical ordering effect in the model therefore arises entirely from the difference in the particle size.

We find that size difference plays a crucial role in the amorphization process. It gives rise to new contributions, such as residual hydrostatic stresses, to the driving force for destabilization of a lattice, which, in turn, are

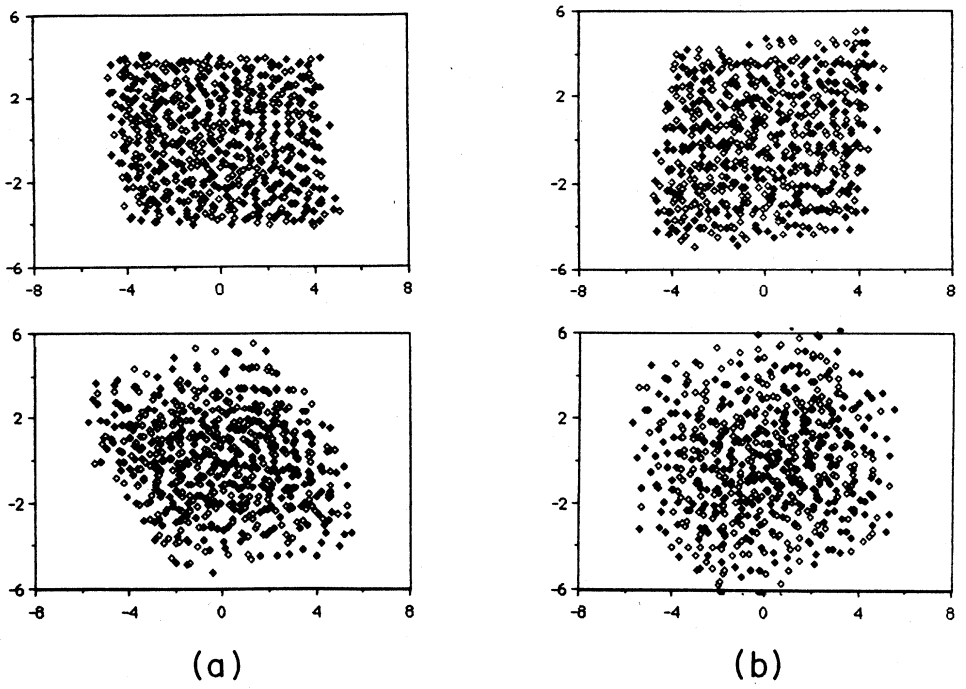

FIG. 15. Same as Fig. 1, except the system is AB solid solution (series D): (a) xy projection and (b) xz projection, and in each case $N_i=0$ (top) and $N_i=40$ (bottom).

responsible for the significantly different threshold conditions for amorphization relative to the single-component lattice. We have found that amorphization of a pure element is dependent on both the rate of defect insertion and the defect concentration.[5,6,9] In the binary solids we find that amorphization is essentially insensitive to the insertion rate, and while the dependence on defect concentration remains the threshold value is appreciably reduced.

For the A_3B ordered lattice amorphization is induced at interstitial concentration of 7.0% but not at 3.5%. The lower concentration, however, is sufficient to cause the transition in the partially disordered AB solid solution. This shows that the structural disordering effects of the interstitials play the same role as the initial structural disorder in the solid.

We have seen that different initial systems give rise to amorphous structures with somewhat different density and internal energy. On the other hand, the elastic constants of the two relaxed amorphous structures, series D and F, are quite similar (cf. Tables II and III).

The present work points out the importance of the relaxation stage in the amorphization process. During this stage there is partial recovery of the density and the internal energy in the case of the A_3B system, while there are large atomic displacements (Fig. 4) and further disordering (Figs. 5 and 6). This behavior is different from

TABLE III. Elastic constants of an amorphized AB solid obtained from simulation series D, stage 4. Contributions from the three terms in Eq. (11)—kinetic, fluctuation, and Born terms, respectively—are shown separately. Shown on the second line of each entry are the corresponding values for the AB lattice without defects, series D, stage 1.

	C_{11}	C_{22}	C_{33}	C_{12}	C_{13}	C_{23}	C_{44}	C_{55}	C_{66}
Kinetic	4.0	4.0	4.0	0	0	0	2.0	2.0	2.0
	4.0	4.0	4.0	0	0	0	2.0	2.0	2.0
Fluctuation	−181	−151	−210	44.1	7.35	40.2	−97.8	−117	−118
	−156	−190	−179	34.8	34.2	82.7	−73.6	−87.1	−118
Born	493	492	500	165	160	164	164	160	165
	464	509	517	177	176	119	119	176	177
Total	315	345	293	209	233	205	68.5	44.3	48.4
	312	322	343	212	211	201	47.0	91.3	61.0
Average		318			216			54	
		326			208			66.4	

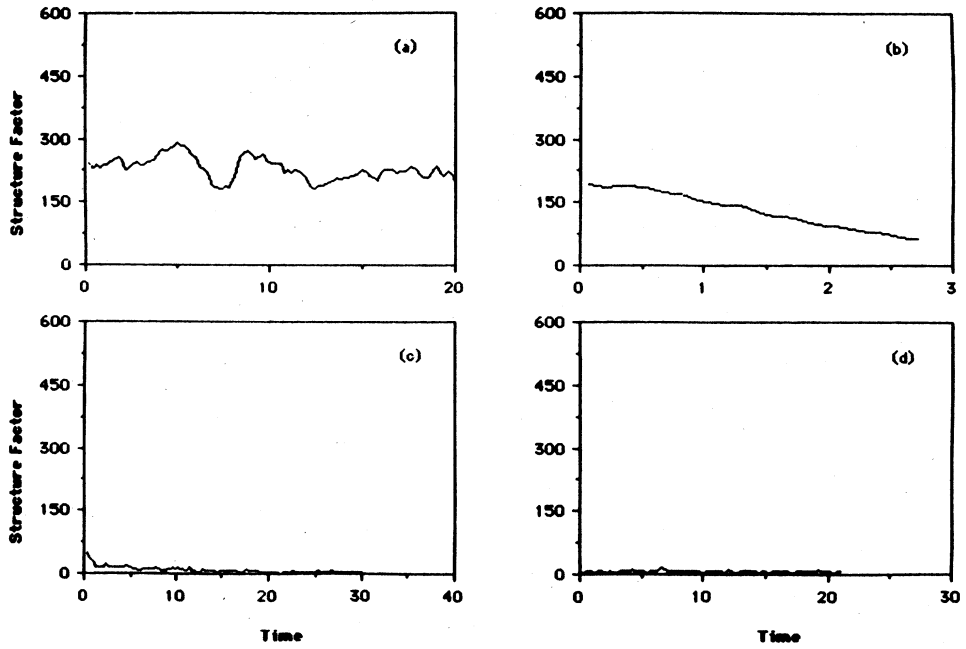

FIG. 16. Same as Fig. 6, except system is AB solid solution.

those during the defect-insertion stage, where loss of order is accompanied by density decrease and energy increase. It is interesting that the average displacements during defect insertion when significant rearrangements are expected to take place turn out to be smaller than those during relaxation. This indicates that at the end of stage 2 the system has not evolved sufficiently to reach its final state. This also suggests that it is possible that systems which have not become amorphous during irradiation may later amorphize during annealing.

The overall behavior of the AB solid solution is in marked contrast to the A_3B ordered lattice, with quite pronounced changes in the latter as amorphization takes place but relatively minor changes in the former. The

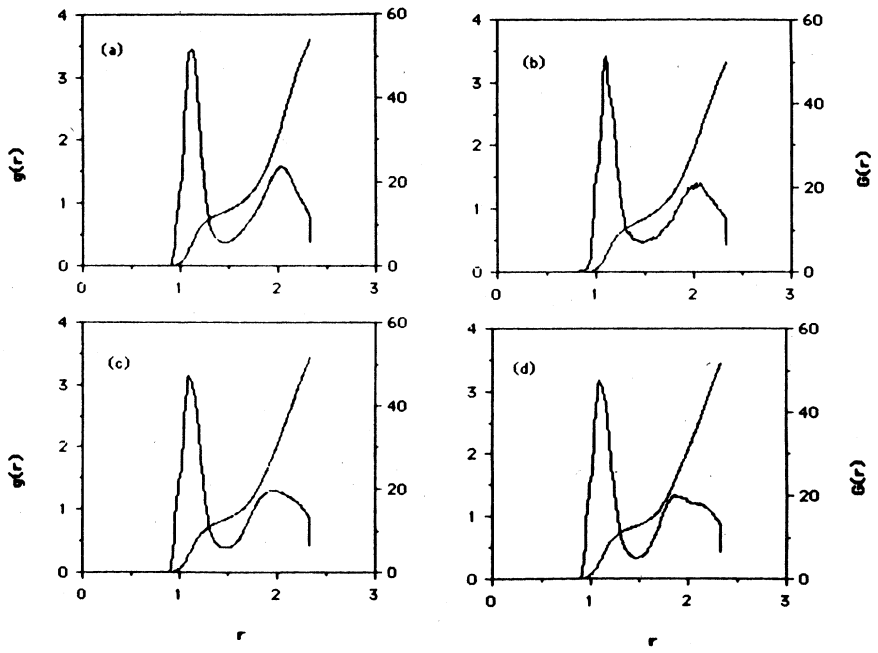

FIG. 17. Same as Fig. 7, except system is AB solid solution.

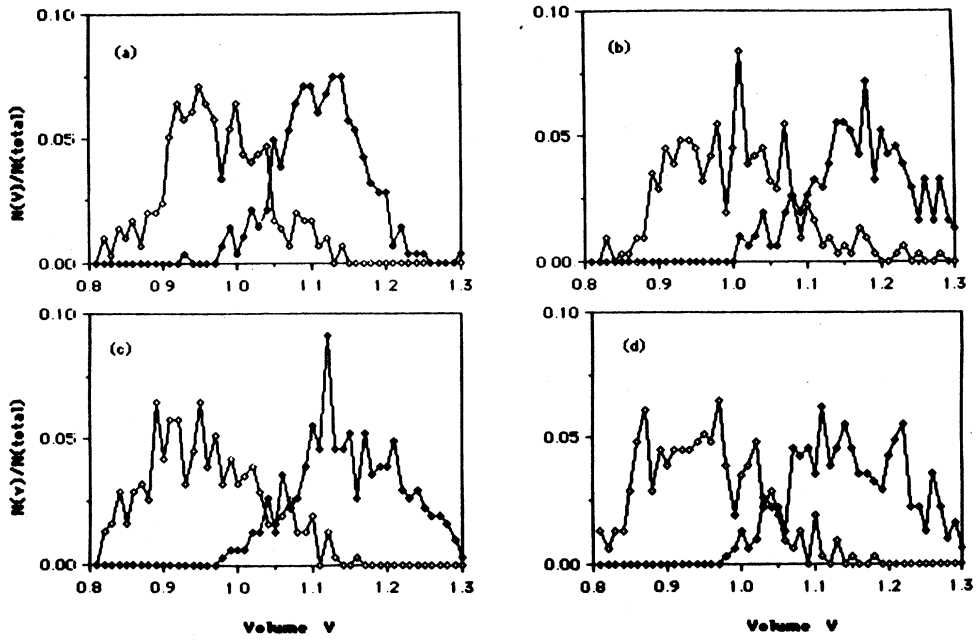

FIG. 18. Same as Fig. 10, except system is *AB* solid solution.

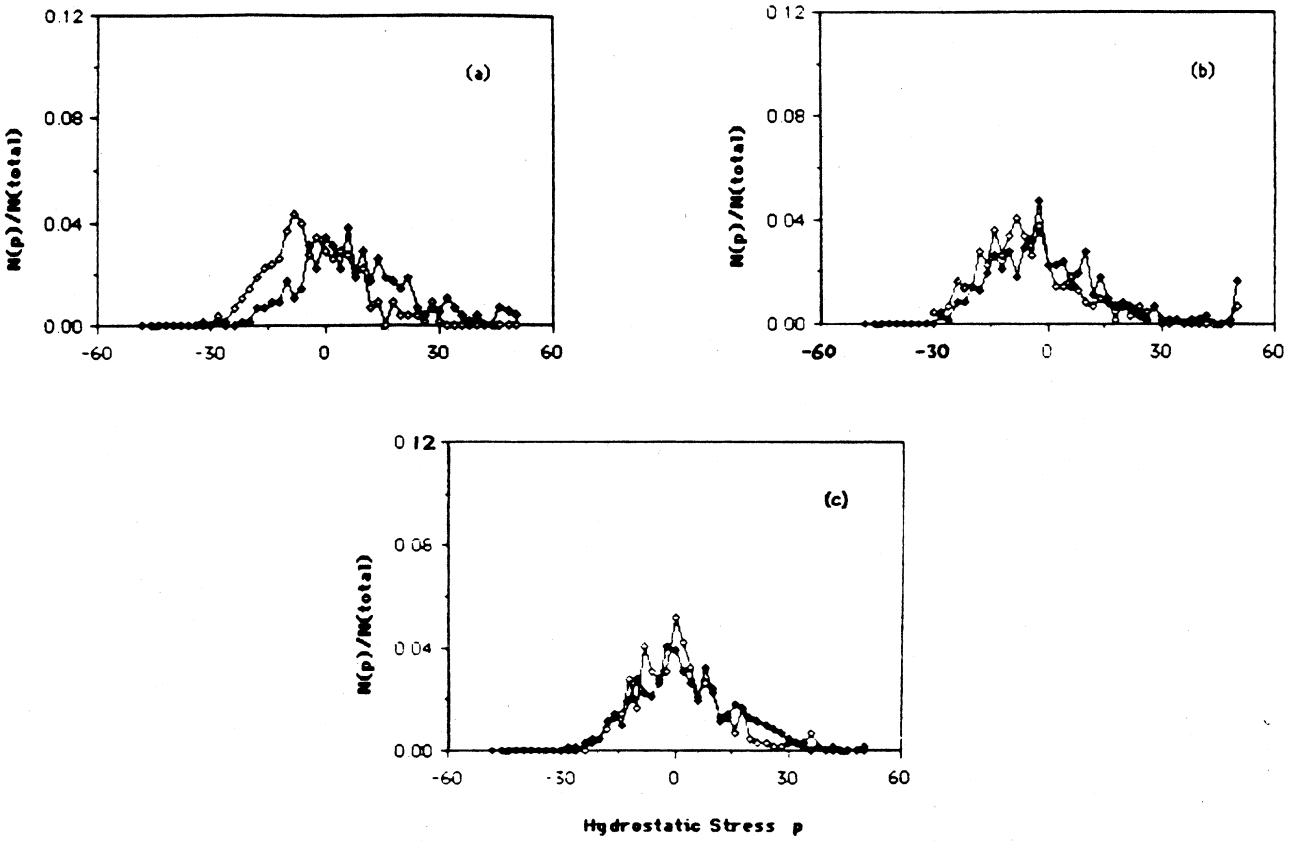

FIG. 19. Same as Fig. 12, except system is *AB* solid solution.

origin of this is clearly the initial disorder that is present in the solid solution. It is also interesting that the amorphous structures produced in both cases have very similar elastic constants.

Since the disorder in the initial AB system arises from the particle-size difference, we see that the nature of this disorder as observed through the various physical properties is the same as that of the disorder produced by the presence of interstitials. In this respect there is no distinction between chemical disorder and structural disorder in the present study.

The present work shows that binary systems are much less resistant to amorphization than monatomic solids. This characteristic of the binary system is well known and is usually attributed to the fact that with two species of the proper size ratio nucleation and recrystallization become more difficult than in the case where all the particles are of the same size.

Recently, it has been reported that hydrogenation is another process which can induce amorphization.[19] Since the hydrogens take up interstitial positions in this case, it would be of interest to look for a connection between our simulations and this type of experiment. A possible difference which should not be overlooked is that in the measurement the interstitials are introduced at the same time and not sequentially as in the simulation. This can lead to different modes of lattice relaxation which could affect the disordering.

There are several directions in which further work would be of interest. A point-defect complex has been proposed as the mechanism for destabilizing the lattice.[11] The validity of this model can be tested by constructing such a complex with proper interatomic potential and carrying out molecular-dynamics runs to determine its stability and influence on structural disordering. It would be useful to continue the study of the effects of chemical ordering by using potential functions with different well depths,[20] and by monitoring the system evolution through the Warren-Cowley and Bragg-Williams order parameters.[21]

ACKNOWLEDGMENTS

One of us (S.Y.) is grateful to the Materials Science Division of Argonne National Laboratory for early support which made this work possible and to our many colleagues there for advice, encouragement, and continued interest, in particular R. S. Averback, N. Q. Lam, P. R. Okamoto, L. E. Rehn, and H. Weidersich. This work has been supported by the U.S. National Science Foundation under Grant No. CHE-84-15078 and No. CHE-88-06767, with computations carried out at the San Diego Supercomputer Center.

*Present address: Department of Materials Science and Engineering, University of Illinois at Urbana-Champaign, Urbana, IL 61801.

[1]R. B. Schwarz and W. L. Johnson, J. Less-Common Met. **140**, 1 (1988); see also other papers in this issue.

[2]D. E. Luzzi and M. Meshii, Res. Mechanica **21**, 207 (1987); D. M. Parkin and R. O. Elliott, J. Mater. Res. **3**, 453 (1988); for a recent discussion of ion-beam mixing, see D. A. Lilienfeld, L. S. Hung, and J. W. Meyer, in Mater. Res. Soc. Bull. **XII**, p. 31 (1987), and related papers in this issue; Y. Limoge and A. Barbu, Phys. Rev. B **30**, 2212 (1984).

[3]C. A. Angell, J. H. R. Clarke, and L. V. Woodcock, Adv. Chem. Phys. **48**, 397 (1981); J. R. Fox and H. C. Andersen, J. Phys. Chem. **88**, 4019 (1984); S. Nosé and F. Yonezawa, Solid State Commun. **56**, 1005 (1985); J. J. Ullo and S. Yip, Phys. Rev. Lett. **54**, 1509 (1985); Phys. Rev. A (to be published); J. G. Amar and R. D. Mountain, J. Chem. Phys. **86**, 2236 (1987).

[4]T. A. Weber and F. H. Stillinger, Phys. Rev. B **32**, 5402 (1985); K. Ding and H. C. Andersen, *ibid.* **34**, 6987 (1986).

[5]Y. Limoge, A. Rahman, H. Hsieh, and S. Yip, J. Non-Cryst. Solids **99**, 75 (1988).

[6]H. Hsieh and S. Yip, Phys. Rev. Lett. **59**, 2760 (1987).

[7]A. Silberstein, P. C. Clapp, and L. E. Tanner, J. Less-Common Met. **140**, 245 (1988).

[8]C. Massobrio, V. Pontikis, and G. Martin (unpublished).

[9]H. Hsieh, Ph.D. thesis, Massachusetts Institute of Technology, 1988.

[10]B. Bernu, J. P. Hansen, Y. Hiwatari, and G. Pastore, Phys. Rev. A **36**, 4891 (1987); R. D. Mountain and D. Thirumalai, *ibid.* **36**, 3300 (1987).

[11]D. F. Pedraza, J. Mater. Res. **1**, 425 (1986); D. F. Pedraza and L. K. Mansur, Nucl. Instrum. Methods B **16**, 203 (1986); D. F. Pedraza, J. Less-Common Met. **140**, 219 (1988).

[12]M. Parrinello and A. Rahman, J. Appl. Phys. **52**, 7182 (1981).

[13]T. Egami, K. Maeda, and V. Vitek, Philos. Mag. A **41**, 883 (1980); T. Egami and D. Srolovitz, J. Phys. F **12**, 2141 (1982).

[14]J. R. Ray, M. Moody, and A. Rahman, Phys. Rev. B **32**, 733 (1985).

[15]J.-P. Boon and S. Yip, *Molecular Hydrodynamics* (McGraw-Hill, New York, 1980).

[16]J. B. Suck, H. Rudin, H. J. Guntherödt, H. Beck, J. Daubert, and W. Glaser, J. Phys. C **13**, L167 (1980); J. B. Suck, H. Rudin, H. J. Guntherödt, and H. Beck, *ibid.* **14**, 2305 (1981).

[17]P. R. Okamoto, L. E. Rehn, J. Pearson, B. Bhadra, and M. Grimsditch, J. Less-Common Met. **140**, 231 (1988).

[18]J. F. Lutsko and D. Wolf (private communication).

[19]W. J. Meng, P. R. Okamoto, L. J. Thompson, B. J. Kestel, and L. E. Rehn, Appl. Phys. Lett. **53**, 1820 (1988).

[20]For a study of compositional order in binary fluid mixture, see R. D. Mountain, Mol. Phys. **59**, 857 (1986).

[21]J. M. Cowley, *Diffraction Physics,* 2nd ed. (North-Holland, Amsterdam, 1981), Chap. 17; L. Guttman, in *Solid State Physics,* edited by F. Seitz and D. Turnbull (Academic, New York, 1956), Vol. 3, p. 145.